ISSN : 0974 - 7486 Volume 12 Issue 8

Materials Science

An Indian Journal

Full Paper

MSAIJ, 12(8), 2015 [269-276]

Study of some characteristics describing the oxidation of a {m, m'}-based {30Cr, 1C, 15Ta} containing alloy during heating up to high temperature and the oxide scales behavior during post-{isothermal stage} cooling. part 2: {m, m'}={Co, Fe}

Kevin Duretz[1,2], Gaël Pierson[1,2], Thierry Schweitzer[2], Elodie Conrath[3], Patrice Berthod[1,2,3]*

[1]University of Lorraine, (FRANCE)

[2]Faculty of Sciences and Technologies, (FRANCE)

[3]Institut Jean Lamour (UMR 7198), Team 206 "Surface and Interface, Chemical Reactivity of Materials"

B.P. 70239, 54506 Vandoeuvre-lès-Nancy, (FRANCE)

E-mail : Patrice.Berthod@univ-lorraine.fr

ABSTRACT

An alloy based on cobalt and iron in equal parts, rich in chromium and containing a dense TaC network in its microstructure was tested in oxidation at high temperature in dry synthetic air. The thermogravimetry tests were performed at 1000, 1100 and 1200°C during 40 hours. The mass gain files were plotted versus temperature and exploited to specify the oxidation start during heating and spallation start during cooling temperatures as well as the successive parts of mass gain achieved during heating and during the isothermal stage. The mass gain kinetic at 1000°C is quite parabolic and the rate rather low. The mass gain curves obtained at 1100 and 1200°C are much more perturbed, with presence of successive high jumps and a tendency to liner oxidation at the end of the isothermal stage. The oxidation start temperature of this CoFe-based alloy was generally lower than for the NiCo-based alloys studied in the first part, and the overall oxidation during heating a little faster. The isothermal mass gain was itself a little higher but the scale spallation behaviour of this CoFe-based alloy during cooling was similar to the NiCo-based alloy one, as is to say not good.

KEYWORDS

Cobalt;
Iron;
Tantalum carbides;
High temperature oxidation;
Oxide spallation.

INTRODUCTION

If cobalt and iron nay be encountered in a same superalloy these two elements are rarely present in the same proportions. One encounter more often cobalt-based superalloys in which iron is also present but in low content, while cobalt may be met in steel but in low quantity.

Many applications involve alloys based on cobalt. Among them one can cite prosthetic dentistry[1] and industrial processes[2,3] working at high temperature, domains in which the chemical resistance brought by the high contents in chromium in these alloys as well as the intrinsic high mechanical resistance of the Co-based

matrix are exploited[4,5]. In case of carbon presence in high concentration the obtained carbides the use may be extended to cutting tools[6] a, d wear-protective coatings[7]. Iron-based alloys, and particularly steels, are widely used in many applications too. Their multiple combinations of chemical compositions and of elaboration conditions (solidification[8], heat-treatment[9]) lead to a wide spectra of properties and then of application as bulk materials[10] or coatings[11].

Between these two important families of alloys there is seemingly no alloys simultaneously based on cobalt and iron. These two very refractory elements (melting point = 1495°C for cobalt and 1535°C for iron) may constitute a very refractory base, refractoriness which can be not really threaten by neither high concentrations in chromium (melting point: 1870°C) nor the presence of tantalum carbides (TaC are among the most stable ones at high temperature). This is the reason why a cast Cr-rich {Co, Fe}-based alloy containing TaC in high fractions was elaborated to first know the development of its microstructure by preliminary thermodynamic calculations and second to metallographically characterize it in its as-cast condition[12]. In the present work it is the behaviour in high temperature oxidation which will be explored.

EXPERIMENTAL

The chemical composition of the studied alloy was initially targeted to be 30wt.%Cr, 1wt.%C, 15wt.%Ta, and equal contents in cobalt and nickel: 27wt.% each of them. As previously specified by Energy Dispersive Spectrometry[12], the obtained composition was 26.41±0.33wt.%Co, 26.79±0.13wt.%Fe, 30.69±0.74wt. %Cr, and 16.11±0.93wt. %Ta (the carbon content being not controllable by EDS). The as-cast microstructure of the alloy is illustrated in Figure 1 by a micrograph taken with a Scanning Electron Microscope (SEM) in Back Scattered Electrons (BSE) mode. The white particles are TaC carbides, the blocky ones of a probably pre-eutectic origin and the script-like ones of an obvious eutectic one. The matrix is composed of two parts: the palest one is probably an austenitic cobalt-iron solid solution containing chromium, and a ferritic darker one containing chromium in especially high content which led to think that it was possibly chromium carbides in a first time[12] (erratum to correct in[12]). Their surface fractions, as measured by image analysis, were 7.55±3.5 surf.% for the ferritic part of matrix and 11.45±1.73 surf.% for the tantalum carbides.

During the cutting performed to obtain the part for the metallographic examinations, three parallelepipeds of about 3mm × 7mm × 7 mm were also prepared, These ones were ground with SiC papers of grade 1200, with smoothing of their edges and corners. The oxidation tests were carried out using a SETARAM TGA92 92-16.18 thermo-balance, with as oxidant atmosphere a flow of dry synthetic air (80%N_2-20%O_2). The heating was realized at +20K min^{-1}, the isothermal stage at 1000, 1100 or 1200°C for 40 hours, and the cooling rate at -5K min^{-1}.

The mass variations were recorded every 32 (test at 1000°C) or 33 (1100&1200°C) seconds. The mass gain files were corrected from the air buoyancy variations and plotted as mass gain versus temperature and exploited to specify the following characteristics:

Heating

- temperature at which the mass gain is significant enough to be detected by the micro-balance,
- eventual determination of the activation energy (if linear part in the curve describing the instantaneous linear mass gain rate variation with temperature, plotted according to the Arrhenius scheme),
- total mass gain achieved during the whole heating between the start of oxidation and the beginning of the isothermal stage),
- final linear mass gain rate when temperature reaches the isothermal stage one;

Isothermal stage

- global shape of the mass gain curve when plotted versus time (parabolic or not, jumps or not),
- total mass gain exclusively achieved during the isothermal stage;

Cooling

- Temperature at which the mass variation accelerates or becomes irregular (start of scale spallation),

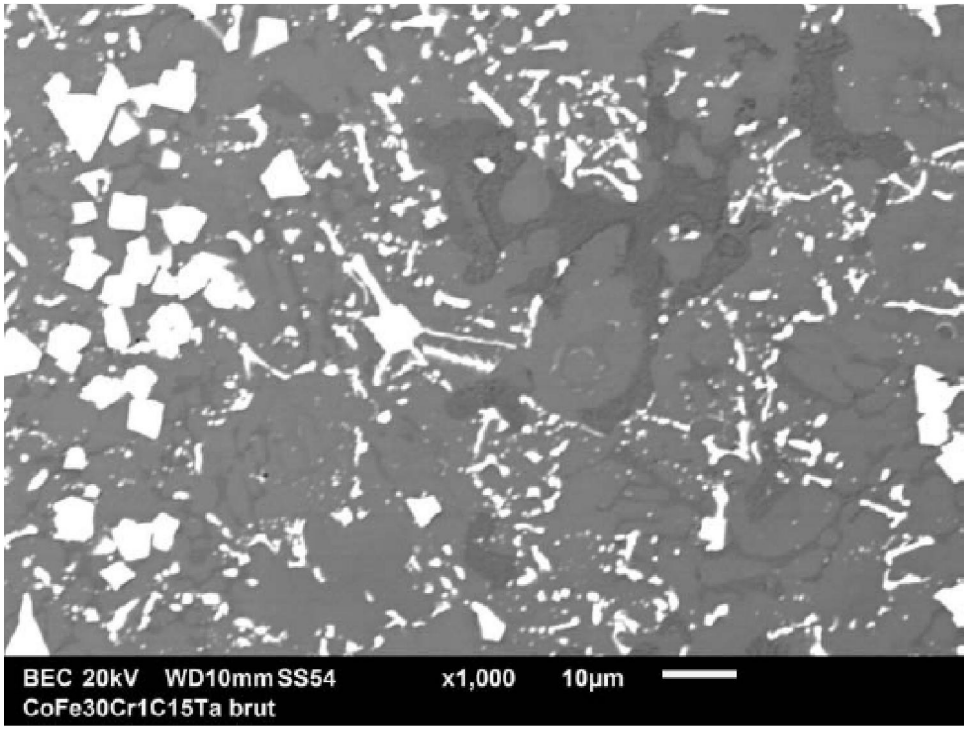

Figure 1 : SEM/BSE micrograph illustrating the as-cast microstructure of the studied alloy

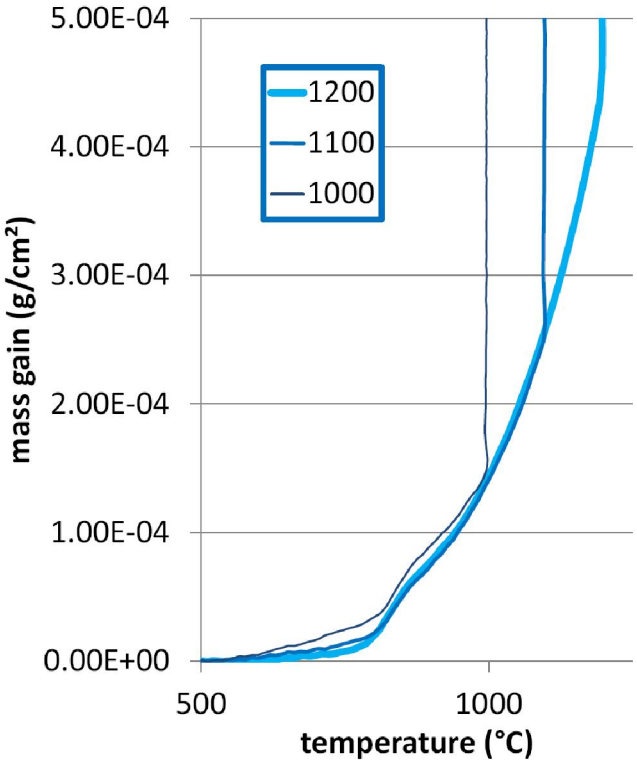

Figure 2 : Enlarged view of the mass gain curves recorded during heating until reaching 1000, 1100 or 1200°C

- final mass variation.

RESULTS AND DISCUSSION

TABLE 1 : Values of the temperatures at which the mass gain by oxidation during heating has become significantly high enough

1000°C-test	1100°C-test	1200°C-test	reproducibility
608.1	767.6	688.4	bad

Oxidation during heating

The heating parts of the mass gain curves plotted versus temperature are presented together in Figure 2. It appears first that the common parts of the 1000°C-curve, the 1100°C-curve and the 1200°C curve (up to 1000°C) are almost superposed; furthermore the common parts of the 1100°C-curve and the 1200°C-one (between 1000 and 1100°C) are strictly the same. However, despite this rather good correspondence between the three curves obtained for the same alloy on the same temperature range (by parts) the temperatures of oxidation start (defined as being the ones at which the mass gain is high enough to be detected by the thermo-balance) are rather scattered (TABLE 1), over the 610-770°C range.

Over these temperatures of oxidation start the instantaneous linear kinetic constant increases more and more rapidly when temperature increases during the heating, this letting thinking here too to an exponential

Full Paper

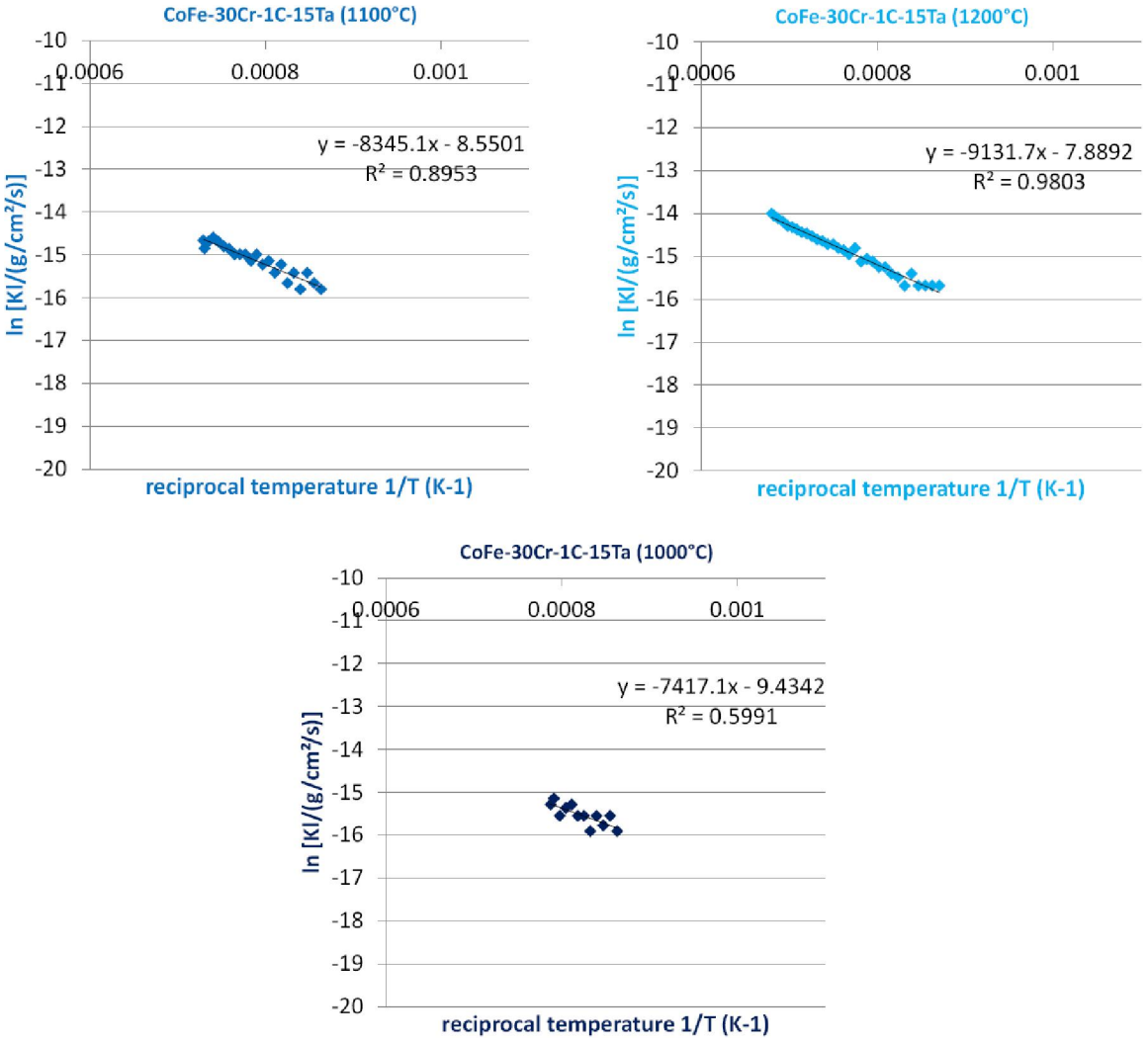

Figure 3 : Arrhenius plot of the instantaneous linear oxidation constant over the whole heating (or only a part if the point's cloud is not straight elongated); values of the slope of the regression straight line for deducing the values of activation energies (displayed in TABLE 2)

TABLE 2 : Values of the activation energies characterizing the dependence on temperature of the linear oxidation constant K_l issued from the successive values of K_l noted during the heating (over the linear part of the Arrhenius plot); value of the K_l value at the start of the isothermal stage

Q (J/Mol) issued from the ln ((dΔm/S)/dt) plot versus 1/T (K) during heating	1000°C-test	1100°C-test	1200°C-test
	61666	69381	75921
Final value of K_l (end of cooling, beginning of the isothermal stage ($\times 10^{-8}$g/cm²/s)	21.25	32.20	78.16
Mass gain at the end of heating (mg/cm²)	0.150	0.262	0.462

increase with temperature. The Arrhenius plot confirms this over the whole heating from oxidation start or only on the high temperature part of the heating, since the points' clouds are globally elongated along a straight line. The slope of the regression straight line led to the values of activation energies listed in the first line of TABLE 2. They are all in the 60-76kJ/Mol range.

The second line of TABLE 2 contains the values of the final value of (dΔm/S)/dt when temperature reaches the stage one. This ultimate value of K_l effectively increases with temperature, showing that oxidation is, at the beginning of the isothermal stage, logically faster when the stabilized temperature is higher.

The mass gains achieved during the whole heating

TABLE 2 : Values of the activation energies characterizing the dependence on temperature of the linear oxidation constant K_l issued from the successive values of K_l noted during the heating (over the linear part of the Arrhenius plot); value of the K_l value at the start of the isothermal stage

Q (J/Mol) issued from the ln ((dΔm/S)/dt) plot versus 1/T (K) during heating	1000°C-test	1100°C-test	1200°C-test
	61666	69381	75921
Final value of K_l (end of cooling, beginning of the isothermal stage ($\times 10^{-8}$g/cm²/s)	21.25	32.20	78.16
Mass gain at the end of heating (mg/cm²)	0.150	0.262	0.462

TABLE 3 : Values of the temperatures at which the mass gain by oxidation during heating has become significantly high enough to be detected by the thermobalance

Oxidation test	Mass gain at the end of heating (mg/cm²); Proportion / heat.+isoth. (%)	Mass gain at the end of the isoth. stage (mg/cm²) (sum of ← and →)	Isothermal mass gain (mg/cm²); Proportion / heat.+isoth. (%)
1200°C-test	0.462 (6.35%)	7.276	6.814 (93.65%)
1100°C-test	0.262 (5.11%)	5.136	4.873 (94.89%)
1000°C-test	0.150 (10.81%)	1.384	1.234 (89.19%)

TABLE 4 : Values of the temperatures at which spallation started during the cooling and final mass variation after return at room temperature

Oxidation test	Temperature of start of the cooling-induced scale spallation (°C)	Final mass variation at the end of the whole thermal cycle (mg/cm²)
1200°C-test	965.9	-1.72
1100°C-test	816.5	-3.78
1000°C-test	602.1	-0.95

are displayed in the third line of TABLE 2. The value is logically higher for a higher temperature.

Isothermal oxidation

When plotted as mass gain versus time the isothermal oxidation curves are not all parabolic. The one obtained for an isothermal stage temperature of 1000°C is effectively really parabolic, with no detectable jumps or tendency to para-linear kinetic. In contrast the mass gain curve obtained for 1100°C is very irregular since affected by many jumps, some of them being rather high. This is also the case for the mass gain curve obtained for 1200°C since two significant jumps are followed by a shape suggesting a kinetic become para-linear. When plotted versus temperature (after having corrected the mass gain files from the air buoyancy variations) the three curves present a first part which quit the abscissa axis leading to the final mass gain already given in the last line of TABLE 2. Thereafter, in this type of representation the oxidation curve becomes a vertical straight line the length of which represents the part of mass gain which is isothermally realized. The values of this isothermal mass gain are given in TABLE 3 (last column). To obtain them the value of the mass gain at the end of the isothermal stage was red in the file and subtracted by the value of the total mass gain achieved during the heating (already given in TABLE 2 but reminded in TABLE 3). Logically the higher the temperature the higher the mass gain achieved during the 40 hours of isothermal oxidation. The calculation of the proportions in TABLE 3 shows that this isothermal mass gain is of course the major part of the total mass gain (89-95%) but it is also true that the mass gain already realized when the isothermal stage starts is significant (5-11% of the final mass gain before cooling).

Phenomena at cooling

The third part corresponds to the cooling during which oxidation may continue but slower and slower. After an eventual jump in mass gain, the mass decreases

rapidly and irregularly: this is the spallation of the external oxide scale which starts at a given temperature and which leads to final mass which may be lower than the previous one if spallation was particularly severe. Sometimes final mass variations may be negative although that the main part of the experiment was characterized by a mass gain all the time before spallation start: the mass of oxygen remaining over the oxidized sample combined with the metallic elements may be lower than the mass of metallic elements lost as oxides when the scale – partly or wholly - quitted the samples. The values of the temperatures at which oxide spallation started during the cooling for the three experiments as well as the final mass variations are given in TABLE 4. It appears that the spallation start temperature increases with the stage temperature.

Graphical summary

The whole curves plotted as mass gain versus temperature are presented in Figure 4 for the 1000°C-case, Figure 5 for the 1100°C-case and in Figure 6 for the 1200°-case, with in each case the designation by arrows of the locations where the values of temperatures or of mass variations were red, as well as the obtained values already presented in the successive tables.

General commentaries

Thus, characterized with the same thermo-balance and for the same conditions of atmosphere and thermal cycle, the present alloys obviously started oxidizing sooner than the NiCo-30Cr-1C-15Ta studied in the first part of this work[13], but with a worse reproducibility for the temperature at which this became detectable during the heating. In contrast the Arrhenius plot of the linear constant during the heating led to the same activation energy for the three tests here while this was not the case for the NiCo-based alloy. At the end of heating the linear constant tended to be slightly higher for the CoFe-based alloy than for the NiCo-based one. Probably due to the lower oxidation start temperatures in the present case (as is to say the sooner mass gain) the mass gain achieved during the whole heating was significantly higher than for the NiCo-based alloys, about three times for the heating up to 1000°C during the first tests and twice for the heatings up to 1100 and 1200°C.

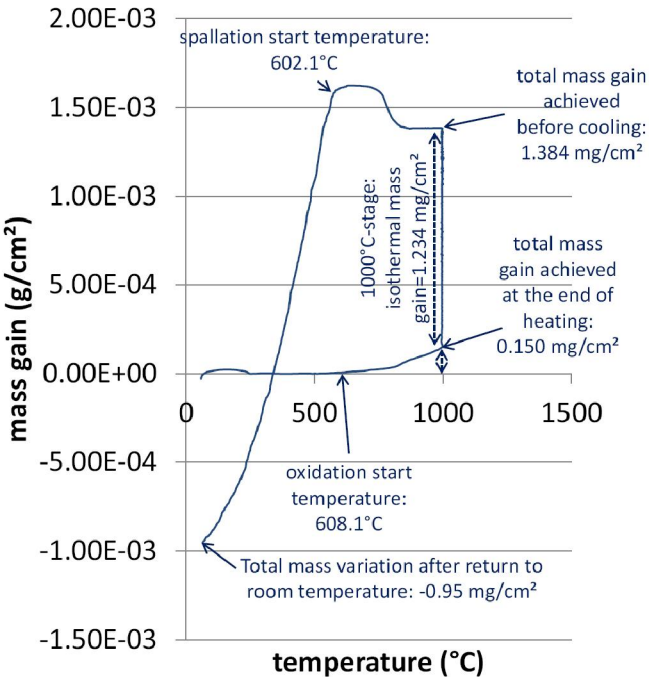

Figure 4 : The {mass gain versus temperature}-plot for the whole thermal cycle of the 1000°C-oxidation test

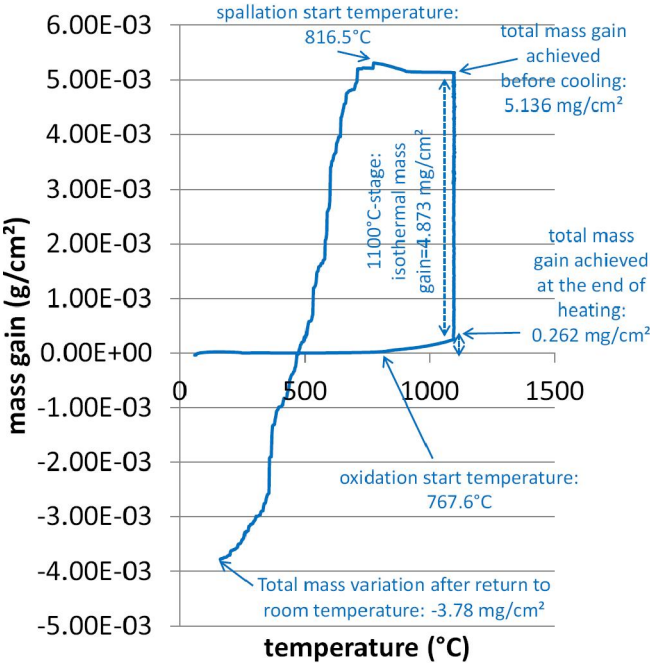

Figure 5 : The {mass gain versus temperature}-plot for the whole thermal cycle of the 1100°C-oxidation test

Consequently the part of the oxidation during heating in the total mass gain just after cooling was here higher than for the Ni-Co-based alloy (6 to 11% instead 4 to 5% for the NiCo-based alloy). The isothermal mass gain were themselves here higher for the same temperature and duration, not really at 1000°C (slow parabolic

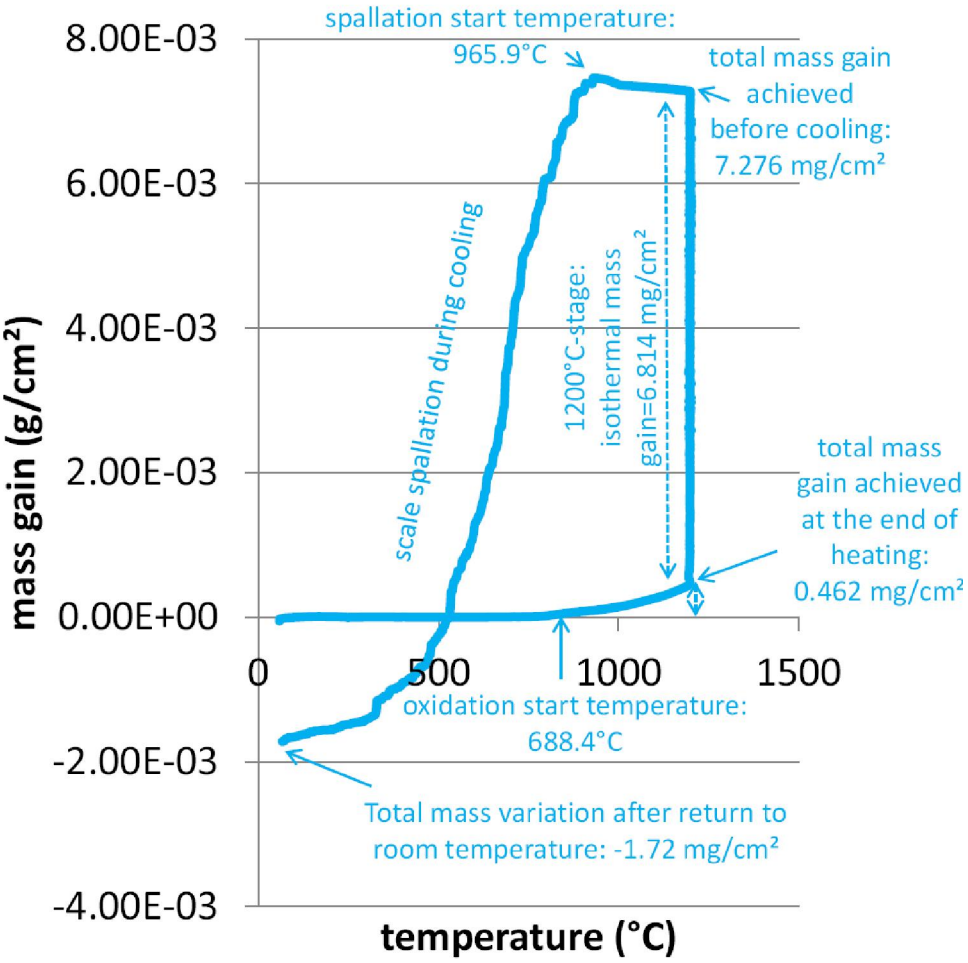

Figure 6 : The {mass gain versus temperature}-plot for the whole thermal cycle of the 1200°C-oxidation test

isothermal kinetic) but significantly at the two other temperatures for which sudden accelerations of mass gain occurred sometimes (jumps). The behaviour of the present CoFe-based alloy during the cooling was globally (by considering the three tests together) not really different from what was observed for the NiCo-based alloy, neither in term of scale spallation start temperature nor final mass after return to room temperature.

CONCLUSIONS

This second 30wt.%Cr-containing TaC-strengthened alloy based on two elements among nickel, cobalt and iron – the CoFe-based one – displayed globally the same type of microstructure as the first alloy, and also a similar behaviour in oxidation at high temperature, despite oxidation rates a little higher. However, if the kinetic was at 1000°C simultaneously purely parabolic and slow, the rather severe scale detachments observed during the isothermal stage at 1100 and 1200°C as well as the start of rapid linear mass gain at the highest temperature demonstrate that this CoFe-based alloy is clearly more threatened by catastrophic oxidation than the NiCo-based one if the temperature is too high. This kinetic study will be soon followed by the post-mortem characterization of the oxidized samples[14] in order to assess their deteriorated states and interpret the oxidation kinetics.

REFERENCES

[1] D.A.Bridgeport, W.A.Brandtley, P.F.Herman; Journal of Prosthodontics, **2**, 144 **(1993)**.
[2] C.T.Sims, W.C.Hagel; "The superalloys", John Wiley & Sons, New York **(1972)**.
[3] P.Berthod, J.L.Bernard, C.Liébaut; Patent WO99/16919.
[4] P.Kofstad; 'High Temperature Corrosion', Elsevier applied science, London **(1988)**.

[5] E.F.Bradley;'Superalloys: A Technical Guide', ASM International, Metals Park **(1988)**.
[6] B.Roebuck, E.A.Almond; Int.Mater.Rev., **33**, 90 **(1988)**.
[7] A.Klimpel, L.A.Dobrzanski, A.Lisiecki, D.Janicki; J.Mater.Process.Tech., **164-165**, 1068 **(2005)**.
[8] K.Kishitake, H.Era, F.Otsubo; Scr.Metall.Mater., **24**, 1269 **(1990)**.
[9] A.Litwinchick, F.X.Kayser, H.H.Baker, A.Henkin; J.Mater.Sci., **11**, 1200 **(1976)**.
[10] H.E.N.Stone; J.Mater.Sci., **14**, 2787 **(1979)**.
[11] B.V.Cockeram; Metall.Trans.A, **33**, 3403 **(2002)**.
[12] G.Pierson, K.Duretz, P.Berthod; Materials Science: An Indian Journal, in press.
[13] G.Pierson, K.Duretz, T.Schweitzer, E.Conrath, P.Berthod; Materials Science: An Indian Journal, submitted.
[14] K.Duretz, G.Pierson, P.Villeger, P.Berthod, E.Conrath; Materials Science: An Indian Journal, to be submitted.